Journal of Energy Storage 52 (2022) 104999

Contents lists available at ScienceDirect

Journal of Energy Storage

journal homepage: www.elsevier.com/locate/est

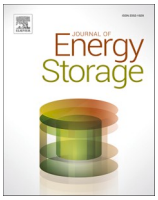

Research papers

An innovative concentrated solar power system driven by high-temperature cascade organic Rankine cycle

Xiao Ren [a], Jing Li [b,*], Guangtao Gao [c], Gang Pei [d]

[a] College of New Energy, China University of Petroleum (East China), Qingdao, China
[b] Research Center for Sustainable Energy Technologies, Energy and Environment Institute, University of Hull, Hull HU6 7RX, UK
[c] The 38th Research Institute of CETC, 199 Xiangzhang Avenue, Hefei, China
[d] Department of Thermal Science and Energy Engineering, University of Science and Technology of China, 96 Jinzhai Road, Hefei, China

ARTICLE INFO

Keywords:
Cascade organic Rankine cycle
Phase change material
Concentrated solar power
Two-tank storage
Saturated steam generation

ABSTRACT

Direct steam generation (DSG) solar power systems eliminate synthetic oils and molten salts in the solar field and enable efficient heat collection. Commercial DSG solar plants usually have a steam generation temperature of 250–285 °C to reduce the technical challenges of wet steam turbines and the costs of high-pressure water storage tanks. The power conversion efficiency is relatively low due to the limited steam generation temperature. This paper proposes a high-temperature solar power system driven by the cascade organic Rankine cycle (CORC). It has three features: water/steam for solar heat transfer, water and phase change material (PCM) for heat storage, and CORC for power conversion. It is the first time that the storage tank temperature is independent of the steam generation temperature in a DSG. Steam can be generated in the solar field at a temperature of 310 °C or even 370 °C. The fundamental of the innovative system is illustrated. The thermodynamic performances during the normal operation and discharge processes are investigated. The results show the maximum thermal efficiency of the CORC system in the normal operation mode is 32.85% at a steam temperature of 311 °C, while the top and bottom cycle efficiencies are 15.38% and 20.86%, respectively. The efficiency increases to more than 37% at 370 °C. Combining the two-tank storage and the PCM unit can overcome the problems of decreasing the heat release rate from PCM during heat discharge while maintaining the CORC system's power output and prolonging the heat storage time. The proposed system is potentially more cost-effective than the existing DSG solar plants.

1. Introduction

Direct steam generation (DSG) is a promising method to reduce the cost of generating electricity from solar thermal power plants [1,2]. In the DSG solar thermal power system, water is used as the working medium for solar collectors, heat storage unit and thermodynamic cycle simultaneously, resulting in a simple system structure and attractive thermo-economic performance [3]. In the early development of the DSG technology, superheated steam Rankine cycles were commonly used, such as in the DISS and INDITEP projects [4]. Later, saturated DSG systems also attracted interest due to the collector field's simple setup (no superheated region), proven safe collector field operation, and higher heat collection efficiency [5]. Common collectors in DSG applications include parabolic trough collector (PTC), linear Fresnel collector (LFC), and solar central tower (SCT). Many saturated DSG plants have been built worldwide [6], and some are listed in Table 1.

These solar plants usually have an operating temperature of 250–285 °C and pressure of 4–7 MPa, which are significantly lower than the temperature and pressure of the plants using thermal oils (e.g., 390 °C/10 MPa) and molten salts (e.g., 560 °C/14 MPa). The saturated steam generated from solar collectors or accumulators is directly injected into the wet steam turbine. The heat-to-power conversion efficiency is therefore lower. Increasing the operating temperature and pressure of the DSG systems could improve the thermodynamic performance, but there are foreseeable limitations and challenges.

First, the wet steam turbine technologies will be more challenging. Commercial DSG plants generally use wet steam turbines for power conversion [7]. In a cascade system, wet steam turbines, including both high-pressure (HP) and low-pressure (LP) ones, are adopted in the saturated DSG plants. They suffer from inefficiency and intense erosion due to the presence of moisture in the expansion process [8]. Under normal circumstances, the wetness of exhaust steam should not be higher than 14% [9,10]. The Baumann rule indicates that a 1%

* Corresponding author.
E-mail address: Jing.Li@hull.ac.uk (J. Li).

https://doi.org/10.1016/j.est.2022.104999
Received 27 March 2022; Received in revised form 20 May 2022; Accepted 27 May 2022
Available online 2 June 2022

Nomenclature

H	enthalpy, kJ
h	enthalpy, kJ/kg
M	mass, kg
$\dot{m}$	mass flow rate, kg/s
Q	heat, W
S	entropy, kJ/K
T	temperature, K
t	operating time, h
W	work, W

Abbreviations

CORC	cascade organic Rankine cycle
DSG	direct steam generation
HTT	high-temperature tank
HP	high-pressure
HX	heat exchanger
LP	low-pressure
LTT	low-temperature tank
ORC	organic Rankine cycle
P	pump
TV	throttle valve
V	valve

Greek letters

α	extracted vapor
ε	machine efficiency
η	efficiency

Subscripts

3rd	third
bot	bottom ORC
CORC	cascade organic Rankine cycle
d	design condition
g	generator
HP	high-pressure
HX	heat exchanger
LP	low-pressure
max	maximum
min	minimum
ORC	organic Rankine cycle
P	pump
pinch	pinch point
r	regenerator
s	isentropic
T	turbine
top	top ORC
water	water

Table 1
Some operational DSG plants worldwide [6].

Project name	Type	Solar field temp. (°C)	Steam pressure (MPa)	Storage duration	Power capacity (MW)
Planta Solar 10	SCT	In:/ out:250+	4.5	1 h Ruths tank	11.0
Planta Solar 20	SCT	In:/ out:250+	4.5	1 h Ruths tank	20.0
eLLO Solar	LFC	In: 190 out:285	7.0	4 h Steam drum	9.0
Puerto Errado 1	LFC	In: 140 out:270	5.5	Ruths tank	1.4
Puerto Errado 2	LFC	In: 140 out:270	5.5	0.5 h Ruths tank	30.0

increment of steam wetness leads to a 1% reduction in turbine efficiency [11]. Fig. 1 shows the enthalpy variations at the outlet of the HP turbine at a given outlet temperature and pressure of 175 °C/0.89 MPa and isentropic efficiency of 0.78. The red and blue dashed lines represent the inlet temperatures of 310 °C and 250 °C, respectively. The outlet wetness doubles with an inlet temperature increment of 60 °C, which is detrimental to the performance of a wet steam turbine.

Second, thermal storage will be infeasible. Steam accumulators are the only commercial solution for the heat storage of DSG solar plants. Current accumulators have a limited storage capacity as the steam pressure falls dramatically with the temperature decrement. To avoid inefficient off-design operation and low power output, the temperature drop during heat discharge is usually less than 50 °C. The lack of long-term and cost-effective storage has restricted the development of DSG technology [12]. Particularly, if the steam temperature and pressure are increased from 250 °C/4 MPa to 310 °C/10 MPa, the thickness of the storage tank will rise three times [13], and will not be economically feasible.

Third, the efficiency increment will be limited. Fig. 2 shows the

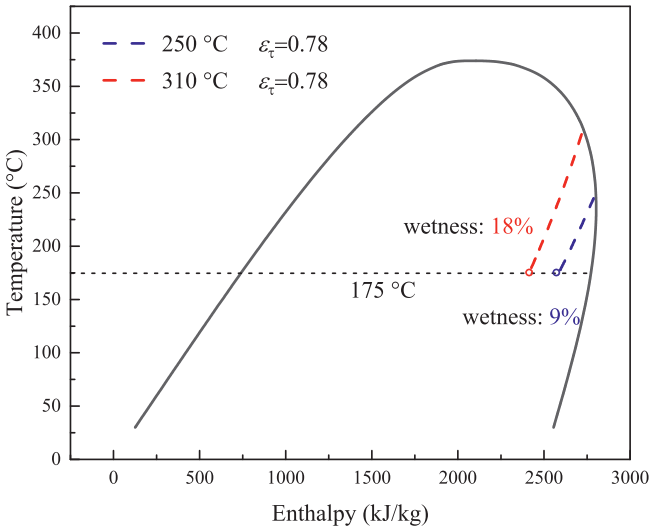

Fig. 1. Increment in the wetness at the outlet of the HP turbine due to a higher inlet temperature of saturated steam.

variations of the equivalent temperature in the heating process [14] and ideal Rankine cycle efficiency with the saturated steam temperature. It is assumed that the solar field inlet temperature is 175 °C. The ideal Rankine cycle efficiency (i.e., no irreversibility during pressurization and expansion) increases from 41.4% to 48.1%. The relative efficiency increment is only 16.2%, while the temperature increment is 100 °C.

The above limitations and challenges can be solved by using the cascade organic Rankine cycle (CORC). Unlike water, the dry organic fluid expands from a saturated vapor state to a superheated state without droplets, thereby providing a safe and efficient expansion process. The organic Rankine cycle (ORC) turbine is a typical dry turbine and has an isentropic efficiency as high as 90% [15], which can overcome the challenges of wet steam turbine technologies. The CORC system has significant heat recovery capacities [16,17] and efficiency promotion

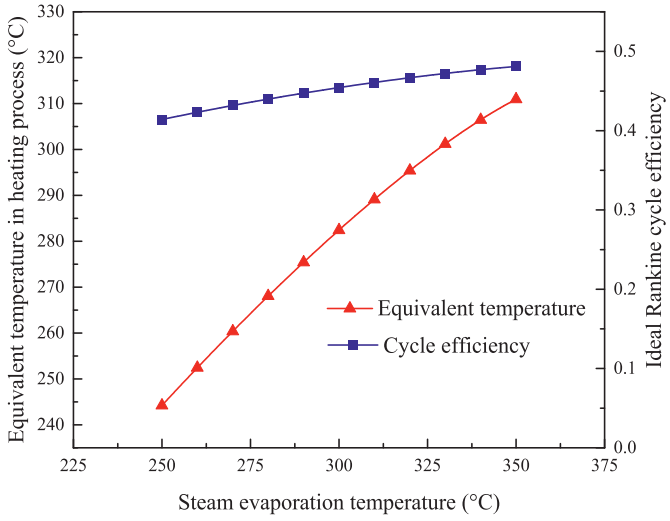

Fig. 2. Variations of the equivalent temperature in the heating process and the cycle efficiency.

potentials [18,19]. The two-stage expansion provides flexibility and has advantages over a single-stage expansion, especially under conditions of fluctuating temperature and heat input [20]. Moreover, the CORC performs better than a parallel two-stage ORC at high heat source temperatures [21]. In recent years, the CORC with two-stage accumulators has attracted increasing interest. However, it is mainly used for waste heat recovery [22–24], liquefied natural gas cold energy recovery [25,26], geothermal power generation [27], and indirect solar thermal power generation without steam generation [28]. There are few reports on the CORC system in the DSG application. The authors proposed a CORC system and found that the system has an efficiency comparable to a traditional DSG system with a lower technical requirement in heat collection and power generation [18,29]. Meanwhile, a need of future work was also outlined.

Phase change material (PCM) provides a higher heat storage capacity and is one of the promising thermal storage technologies. Compared to sensible heat storage, PCM has a significantly higher energy density and requires a relatively smaller size [30,31]. Gang et al. [32] proposed a solar ORC system with a PCM heat storage unit, which can achieve a higher temperature. Freeman et al. [33] applied PCM storage in a small-scale ORC system. The isothermal operation of the PCMs made a smaller storage temperature fluctuation and higher energy conversion efficiency. Laing et al. [34] proposed a three-part storage system combining PCM modules for two-phase evaporation and concrete modules for water preheating and steam superheating. However, a major barrier of PCM in the DSG application is that during the discharge process, solid PCM, which has a low thermal conductivity, freezes on the heat transfer surface leading to a large increment in the thermal resistance [35]. The heat exchangers have a limited area for cost-effectiveness. As more PCM solidifies on the heat exchanger surface, it is difficult to maintain a constant steam evaporation temperature and a high heat release rate simultaneously. The decrement in either the steam temperature or heat release rate will reduce the output and efficiency of the power cycle.

This paper proposes a novel high-temperature solar CORC power generation system to tackle the above challenges. It aims to elevate the steam generation temperature and enlarge the storage capacity. Unlike a conventional DSG system, the operation temperature of the water storage tank is independent of the steam generation temperature. The latter can reach 310 °C or even 370 °C with a high heat-to-power conversion efficiency, while the former is about 250 °C with a relatively low water tank cost. Moreover, two-tank water storage is innovatively combined with the PCM unit. Both sensible heat from hot water and latent heat from the PCM are used to drive the power cycle in the discharge process. The sensible heat increases with the decrement in the heat release rate from the PCM, thereby overcoming the major barrier of PCM in the DSG applications and maintaining a high level of power generation during discharge. The logic diagram of this paper is shown in Fig. 3. The design and principle of the solar CORC power generation system combined with sensible and latent heat storage are illustrated in Section 2, and mathematical models are built in Section 3. A close view to the performance in the charge and discharge processes is presented in Section 4. A comparison between the proposed system and the common DSG and

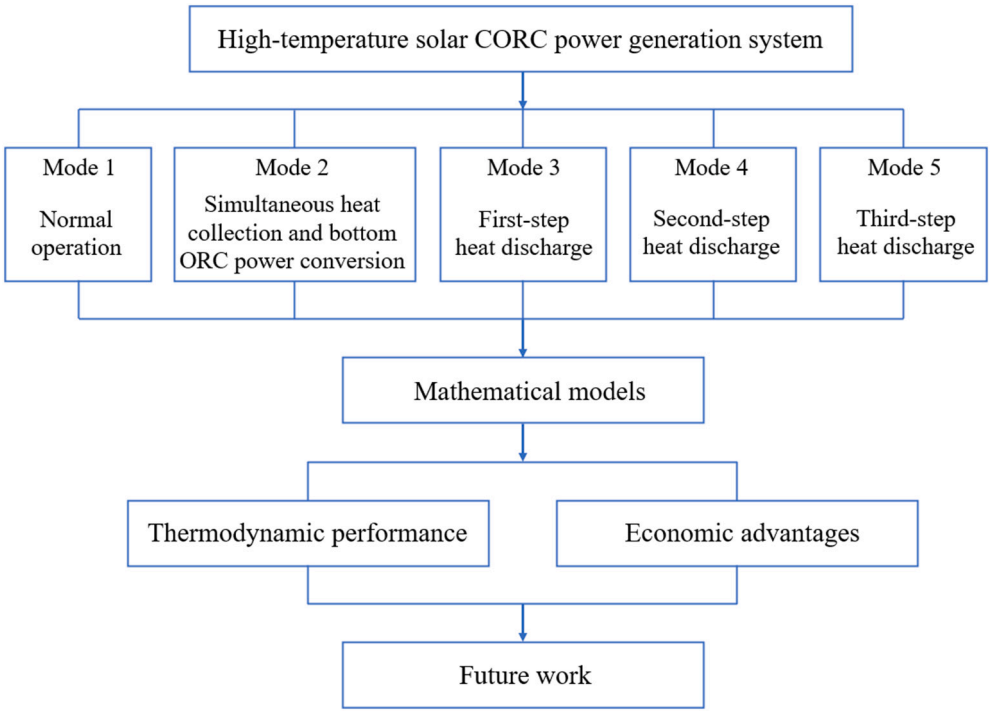

Fig. 3. Logic diagram of this paper.

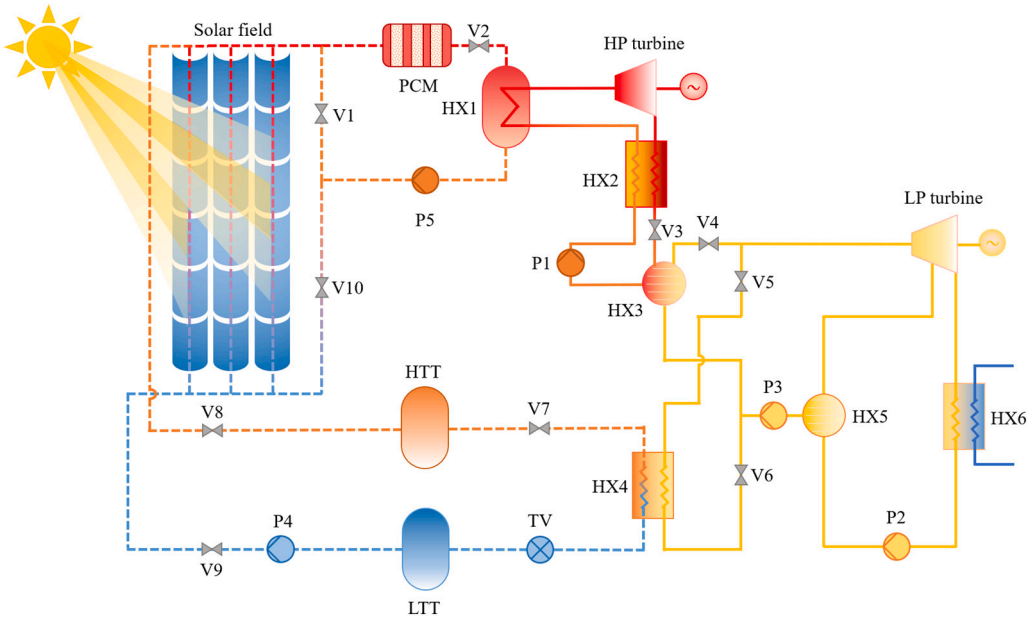

Fig. 4. Structure diagram of the CORC system.

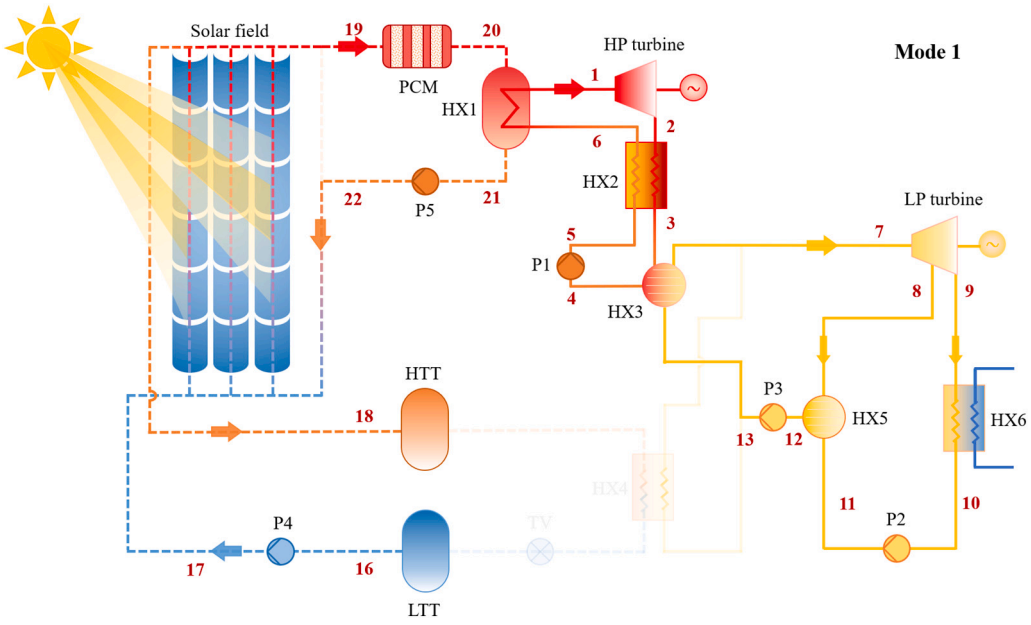

Fig. 5. Mode 1 - normal operation.

solar ORC systems is made in Section 5, followed by an outline for future research in Section 6.

2. System description

Fig. 4 shows the schematic diagram of the proposed CORC system combined with sensible and latent heat storage, which consists of three subsystems: solar field, storage units and cascade ORC. The solar field subsystem can be either parabolic trough collectors, Fresnel reflectors or central tower receivers. The solar field can be divided into different loops. Some loops are used to generate steam for power conversion and charge the PCM, while other loops are used to heat water for the high-temperature tank (HTT). The top ORC is connected to the solar field directly and coupled with the bottom ORC unit through a mixing chamber (HX3). It comprises a PCM module, high-pressure (HP) turbines, pumps, evaporators (HX1), an internal heat exchanger (HX2), and a condenser (mixing chambers HX3). The PCM may have a melting point of higher than 311 °C. The bottom ORC comprises of an HTT and a low-temperature tank (LTT) which are connected to the solar field, low-pressure (LP) turbines, evaporators (HX3 or HX4), feed-fluid heater (mixing chambers HX5), and condenser (HX6). The HTT may have a design temperature of about 250–285 °C for the sake of cost-effectiveness. For the bottom ORC, the evaporator and condenser are HX3 and HX6 respectively, when the system works in the normal mode. The evaporator can be HX3 or HX4 or both during heat discharge.

According to the direct normal irradiance (DNI), the system can operate in five modes, including normal operation (Mode 1), simultaneous heat collection and bottom ORC power conversion (Mode 2), first-step heat discharge (Mode 3), second-step heat discharge (Mode 4), and third-step heat discharge (Mode 5). The details are as follows:

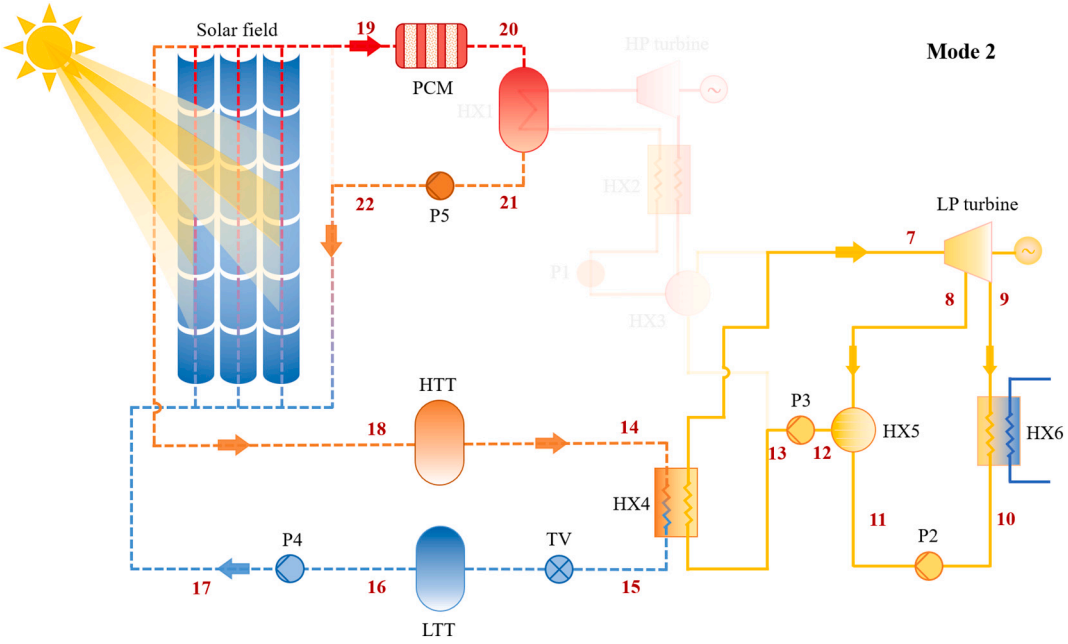

Fig. 6. Mode 2 - simultaneous heat collection and bottom ORC power conversion.

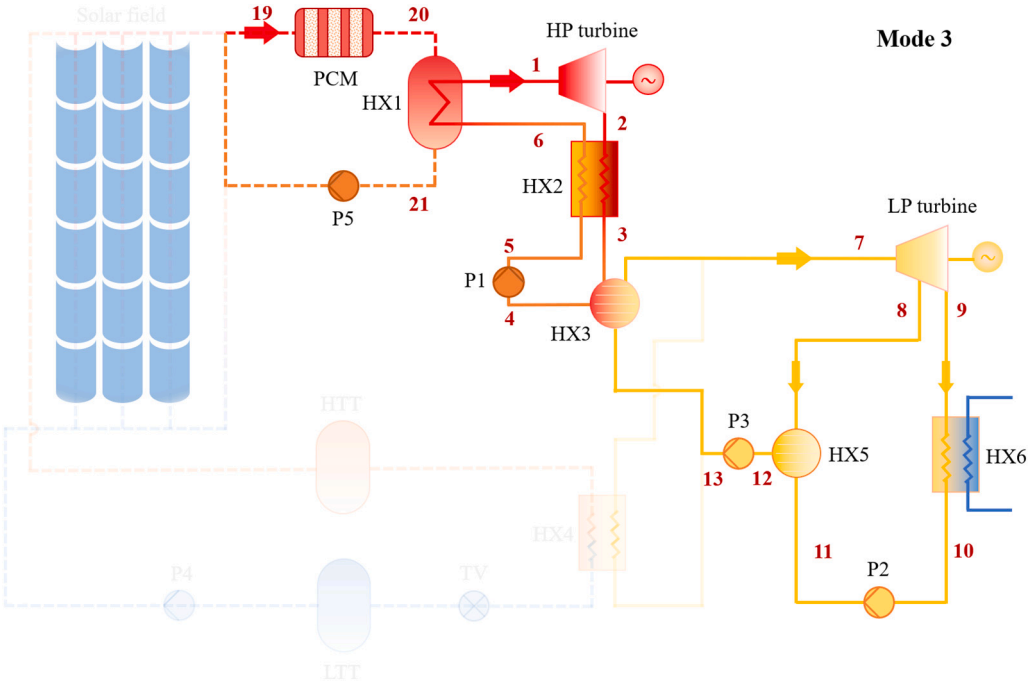

Fig. 7. Mode 3: first-step heat discharge.

(1) Mode 1. The solar heat collection and CORC power conversion take place simultaneously, as shown in Fig. 5. The system operates in this normal mode when solar irradiance is relatively strong (e.g., DNI >450 W/m^2). Power is produced through CORC. All the pumps and turbines are operational. Water mass flow rates through P4 and P5 are adjustable to guarantee steady power conversion of the CORC. The solar heat is more than that consumed by the CORC. The residual solar heat is stored in the PCM and HTT. The saturated steam is used to evaporate the organic fluid in HX1. The saturated organic vapor expands in the HP turbine. Exhaust vapor at the superheated state is precooled in the HX2 and condensed into liquid or cooled down through the mixing chamber (HX3). The organic fluid from P3 is heated by the exhaust vapor from the HP turbine. The saturated vapor in HX3 flows into the LP turbine to generate power, part of which is extracted to preheat the liquid from P2. On the completion of this mode, PCM is charged and most water accumulates in the HTT.

(2) Mode 2. Simultaneous heat collection and bottom ORC power conversion may happen when solar radiation is relatively weak (e.g., in the early morning or late afternoon), as shown in Fig. 6. The throttle valve TV is open and the pump P2, P3, P4, and P5 are operational. The solar heat is less than the rated heat input to the

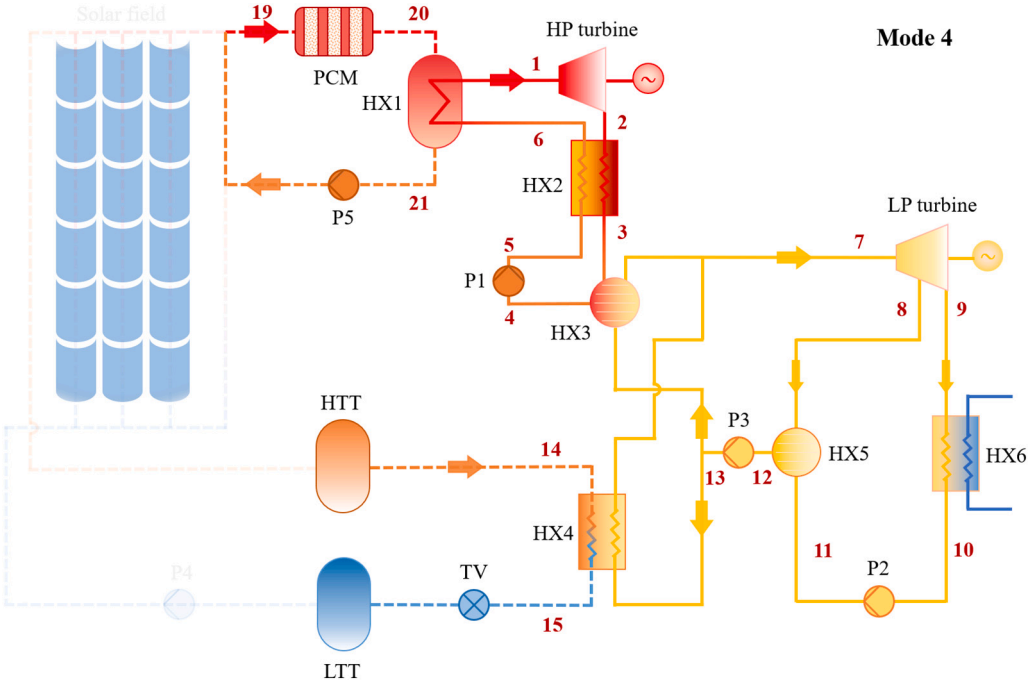

Fig. 8. Mode 4: second-step heat discharge.

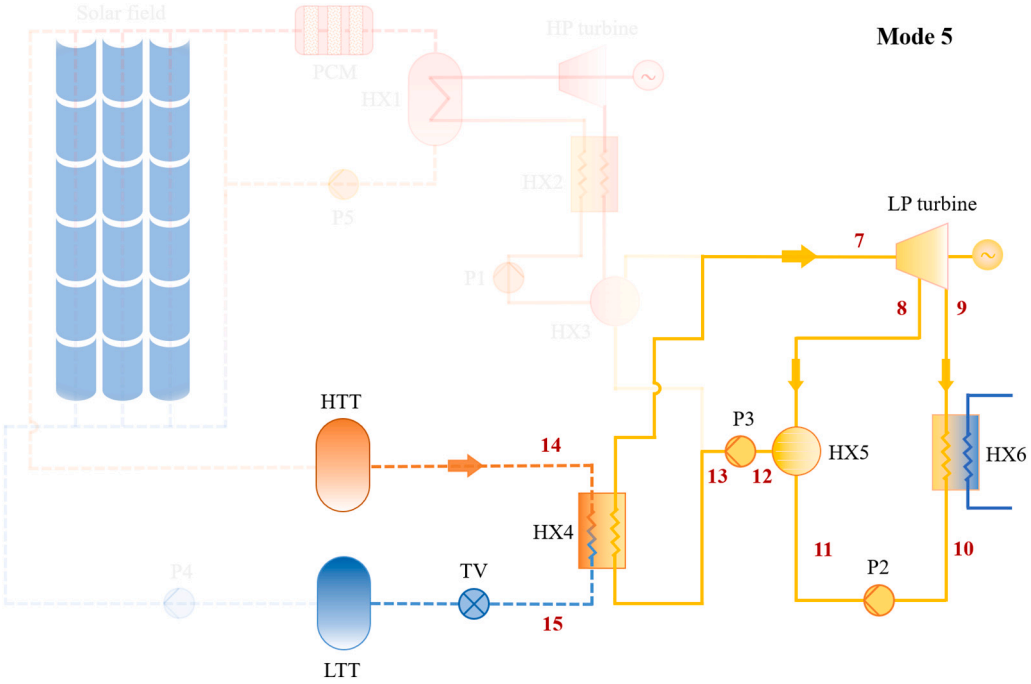

Fig. 9. Mode 5: third-step heat discharge.

CORC. In this mode, the PCM and HTT are partially charged. The top ORC does not work.

(3) Mode 3. In the first step of heat discharge, the latent heat is released from the PCM to drive the CORC, as shown in Fig. 7. The pumps P1, P2, P3, and P5 are operational. The power conversion is similar to that in normal operation. However, the evaporation temperature of the organic fluid is likely to decrease due to the increased thermal resistance in the PCM solidification process.

(4) Mode 4. To prevent a significant drop of the CORC power output, the water in the HTT flows into the LTT as described by the second-step heat discharge in Fig. 8. Both latent heat from the PCM and sensible heat from the HTT are employed to drive the power cycle. The throttle valve TV is open and the pumps P1, P2, P3, and P5 are operational. Aside from the mixing chamber, HX4 provides additional heat to the bottom ORC. HX4 can work with HX3 in parallel. One stream of ORC fluid is vaporized by HX3, and the other is vaporized by HX4. Water flows to the LTT, leading to a mass reduction in the HTT. The flow rate is

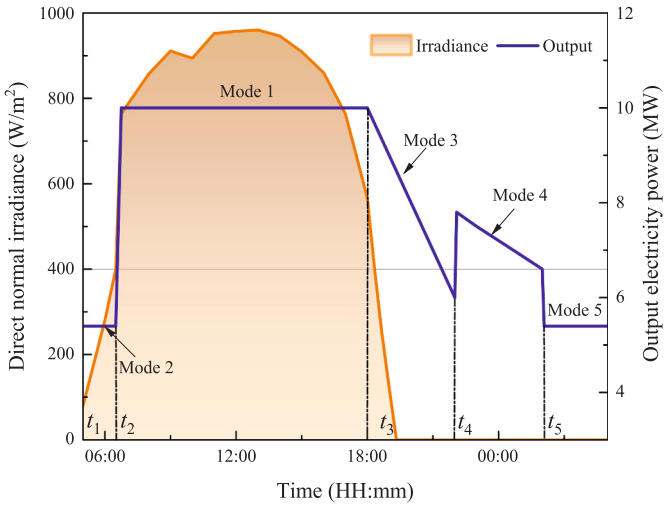

Fig. 10. Variations of the operation mode throughout a typical day.

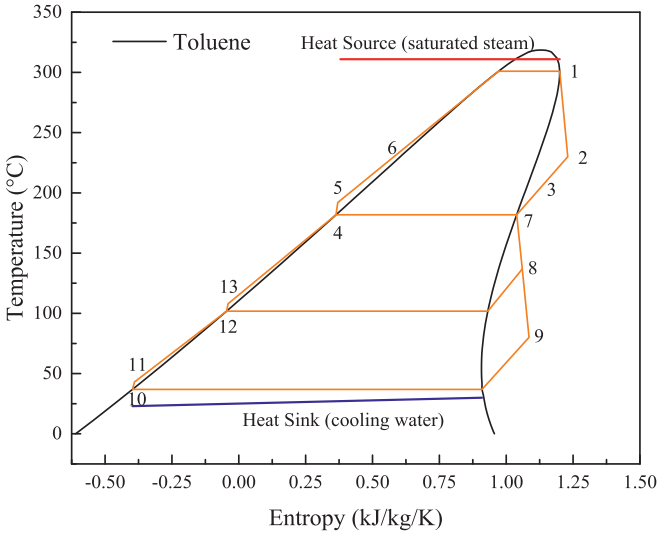

Fig. 11. T-s diagram of the CORC system under Mode 1.

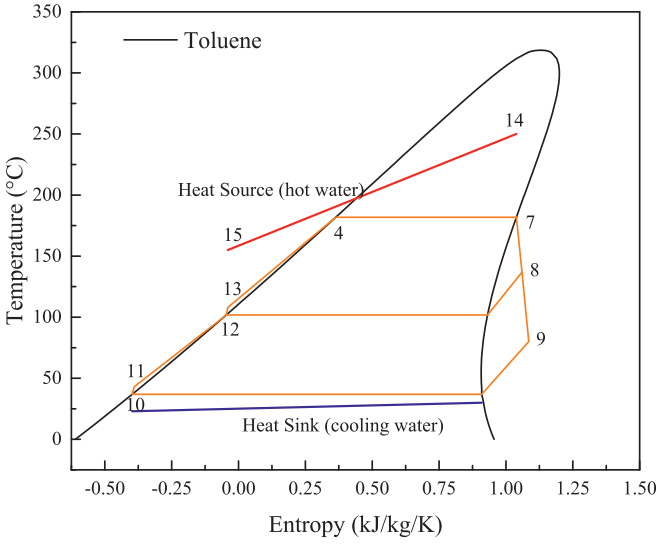

Fig. 12. T-s diagram of the CORC system under Mode 5.

controllable. HX4 helps compensate for the heat shortage from the PCM and guarantees the normal operation of the bottom ORC. This mode comes to an end when the PCM is fully discharged.

(5) Mode 5. In the third step of heat discharge, the water in the HTT flows to the LTT and the heat is used to drive the bottom ORC, as shown in Fig. 9. The throttle valve (TV) is open and the pump P2 and P3 are operational. The power conversion in this mode is stable.

The power output on a typical sunny day is illustrated in Fig. 10. The operation period of Mode 1 is from t2 to t3, and it is from t1 to t2 for Mode 2, t3 to t4 for Mode 3, t4 to t5 for Mode 4, and t5 to t1 for Mode 5. It is assumed that the rated power output is 10 MW. There is a jump in the power output at t4 when the water in the HTT flows into the LTT with heat input to HX4, and the LP turbine shifts from the off-design to normal operation. A drop also exists at t5 when the heat release from the PCM is completed or the top ORC stops to avoid inefficient part-load operation.

The proposed system is flexible and can react to fluctuating solar radiation. There are more advantages as follows:

First, it tackles the challenge of wet steam turbines associated with conventional DSG systems and is able to operate at a much higher temperature and pressure. The water/steam in the novel system is not the working fluid of the power cycles, and the wet steam turbines are eliminated. The water/steam temperature from the solar field can reach 300–370 °C, accompanied by a high evaporation temperature of the ORC fluid. Therefore, the power cycle efficiency in the normal operation is significantly higher than that of a conventional DSG system.

Second, it overcomes the barrier of heat storage for the DSG technology. The two-tank water storage is independent of the top cycle. The temperature of the water tanks can be lower than 250 °C even though the tope cycle operates at 300–370 °C, leading to cost-effective sensible heat storage.

Third, the combination of sensible and latent heat storage overcomes the shortage of the PCM. As shown in Mode 4 in Fig. 8, when the heat discharge rate of the PCM decreases during solidification, the sensible heat released by the water is increased to guarantee the normal operation of the bottom ORC, thereby enabling a high level of the power output of the CORC.

3. Mathematical models

In modeling the novel CORC system, emphasis will be put on the heat-to-power conversion in the five modes. The power conversion of the bottom ORC in Mode 2 is the same as that in Mode 5. Power conversion in Mode 3 and Mode 4 is the off-design process. The thermodynamic processes for Mode 1 and Mode 5 are shown in Figs. 11 and 12 by taking toluene as the CORC fluid. It has a boiling point of 111 °C, a critical temperature of 318.6 °C, and critical pressure of 4.1 MPa. The numbers indicate the thermodynamic states of water and organic fluid that correspond to the marks in Figs. 5 and 9. The heat and friction loss in the pipes and heat exchangers are ignored. The changes in kinetic and potential energy are disregarded in the simulation.

3.1. Turbines

The work generated by the top ORC turbine and bottom ORC turbine is calculated by

$$W_{HP} = \dot{m}_{ORC,top}(h_1 - h_2) = \dot{m}_{ORC,top}(h_1 - h_{2s})\varepsilon_T \quad (1)$$

$$W_{LP} = \dot{m}_{ORC,bot}[\alpha(h_7 - h_8) + (1-\alpha)(h_7 - h_9)] = \dot{m}_{ORC,bot}[\alpha(h_7 - h_{8s})\varepsilon_T + (1-\alpha)(h_7 - h_{9s})\varepsilon_T] \quad (2)$$

where ε_T is the isentropic efficiency of the top and bottom ORC turbine; $\dot{m}_{ORC,top}$ and $\dot{m}_{ORC,bot}$ are the mass flow rate of the top and bottom ORC (kg/s); h is the enthalpy value of each point (kJ/kg); α is the fraction of the flow rate that goes into the regenerator from the turbine and expressed as

$$\alpha = (h_{12} - h_{11})/(h_8 - h_{11}) \quad (3)$$

The ratio of the off-design mass flow rate to the design mass flow rate can then be calculated by [36]

$$\frac{\dot{m}}{\dot{m}_d} = \sqrt{\frac{T_d}{T}}\sqrt{\frac{p_1^2 - p_2^2}{p_{d1}^2 - p_{d2}^2}} \quad (4)$$

where $\dot{m}$ and T are the mass flow rate (kg/s) and temperature (K) of the turbine at the off-design condition; the $\dot{m}_d$ and T_d are the mass flow rate (kg/s) and temperature (K) of the turbine at the design condition; p_{d1} and p_{d2} are the pressure of the inlet and outlet turbine at the design condition (Pa); p_1 and p_2 are the pressure of the inlet and outlet turbine at the off-design condition (Pa).

3.2. Heat exchangers

The heat balances in HX2, mixing chamber HX3, HX4 are determined by

$$\dot{m}_{ORC,top}(h_2 - h_3) = \dot{m}_{ORC,top}(h_6 - h_5) \quad (5)$$

$$\dot{m}_{ORC,top}(h_3 - h_4) = \dot{m}_{ORC,bot}(h_7 - h_{13}) \quad (6)$$

$$\dot{m}_{water,bot}(h_{14} - h_{15}) = \dot{m}_{ORC,bot}(h_7 - h_{13}) \quad (7)$$

where $\dot{m}_{water,bot}$ is the mass flow rate of the bottom water cycle (kg/s).

3.3. Pump

The work required by the pumps P1, P2, P3, and P4 is determined by

$$W_{P1} = \dot{m}_{ORC,top}(h_5 - h_4) = \dot{m}_{ORC,top}(h_{5s} - h_4)\Big/\varepsilon_P \quad (8)$$

$$W_{P2} = \dot{m}_{ORC,bot}(1-\alpha)(h_{11} - h_{10}) = \dot{m}_{ORC,bot}(1-\alpha)(h_{11s} - h_{10})\Big/\varepsilon_P \quad (9)$$

$$W_{P3} = \dot{m}_{ORC,bot}(h_{13} - h_{12}) = \dot{m}_{ORC,bot}(h_{13s} - h_{12})\Big/\varepsilon_P \quad (10)$$

$$W_{P4} = \dot{m}_{water,bot}(h_{17} - h_{16}) = \dot{m}_{water,bot}(h_{17s} - h_{16})\Big/\varepsilon_P \quad (11)$$

where ε_P is the isentropic efficiency of the working fluid pump.

3.4. Thermal efficiency

The heat transferred to the working fluid in the evaporators of the top ORC and bottom ORC is calculated by

$$Q_{ORC,top} = \dot{m}_{ORC,top}(h_1 - h_6) \quad (12)$$

$$Q_{ORC,bot} = \dot{m}_{ORC,bot}(h_7 - h_{13}) \quad (13)$$

$$Q_{water,bot} = \dot{m}_{water,bot}(h_{14} - h_{15}) \quad (14)$$

The work of the top ORC, bottom ORC, and CORC in Mode 1 is expressed as

$$W_{ORC,top} = W_{HP}\varepsilon_g - W_{P1} \quad (15)$$

$$W_{ORC,bot} = W_{LP}\varepsilon_g - W_{P2} - W_{P3} \quad (16)$$

$$W_{CORC} = (W_{HP} + W_{LP})\varepsilon_g - W_{P1} - W_{P2} - W_{P3} \quad (17)$$

where ε_g is the generator's efficiency.

The thermal efficiencies of the top ORC, bottom ORC, and CORC in Mode 1 and Mode 3 are expressed as

$$\eta_{ORC,top} = W_{ORC,top}/Q_{ORC,top} \quad (18)$$

$$\eta_{ORC,bot} = W_{ORC,bot}/Q_{ORC,bot} \quad (19)$$

$$\eta_{CORC} = W_{CORC}/Q_{ORC,top} \quad (20)$$

The work and thermal efficiency of the bottom ORC in Mode 2 and Mode 5 are expressed as

$$W_{ORC,3rd} = W_{LP}\varepsilon_g - W_{P2} - W_{P3} - W_{P4} \quad (21)$$

$$\eta_{ORC,3rd} = W_{ORC,3rd}/Q_{ORC,bot} \quad (22)$$

The thermal efficiency of the CORC system in Mode 4 is expressed as

$$\eta_{CORC,2rd} = W_{CORC}/(Q_{ORC,top} + Q_{water,bot}) \quad (23)$$

3.5. Heat storage capacity

For a certain amount of storage water, the runtime of the bottom ORC in Mode 5 is expressed as

$$t_{ORC,3rd} = M_w\Big/\dot{m}_{water,bot} \quad (24)$$

The heat storage capacity is calculated as

$$W_{3rd} = t_{ORC,3rd}W_{ORC,3rd} \quad (25)$$

3.6. Entropy generation

The entropy generation in the ORC turbines, heat exchangers, and pumps represents the thermodynamic irreversibility in each component. The entropy generation of the HP turbine and LP turbine is expressed as

$$\Delta S_{HP} = S_2 - S_1 \quad (26)$$

$$\Delta S_{LP} = \alpha S_8 + (1-\alpha)S_9 - S_7 \quad (27)$$

The entropy generation of the HX1, HX2, mixing chamber HX3, HX4 is determined by

$$\Delta S_{HX1} = S_1 - S_6 - (H_1 - H_6)/T_{heat} \quad (28)$$

$$\Delta S_{HX2} = S_6 - S_5 + S_3 - S_2 \quad (29)$$

$$\Delta S_{HX3} = S_4 - S_3 + S_7 - S_{13} \quad (30)$$

$$\Delta S_{HX4} = S_{15} - S_{14} + S_7 - S_{13} \quad (31)$$

$$\Delta S_{HX5} = S_{12} - (\alpha S_8 + (1-\alpha)S_{11}) \quad (32)$$

$$\Delta S_{HX6} = S_{10} - S_9 - (H_{10} - H_9)/T_{cool} \quad (33)$$

The entropy generation of the pump P1, P2, P3, and P4 is calculated as

$$\Delta S_{P1} = S_5 - S_4 \quad (34)$$

$$\Delta S_{P2} = S_{11} - S_{10} \quad (35)$$

$$\Delta S_{P3} = S_{13} - S_{12} \quad (36)$$

Table 2
Some specific parameters in the simulation.

Parameter	Value
Rated output power of CORC system, W_{CORC} (MW)	10
Operating time of CORC, t_{CORC} (h)	8
ORC turbine isentropic efficiency, ε_T	85%
Pump isentropic efficiency, ε_P	80%
Generator efficiency, ε_g	95%
Regenerator efficiency (HX2), ε_r	70%
Ambient temperature, T_a (°C)	20
Bottom ORC condensation temperature, T_{10} (°C)	30
Temperature of hot water stored in HTT, T_{14} (°C)	250
Minimum temperature difference, ΔT_{min} (°C)	10
Water mass of HTT, (ton)	1500

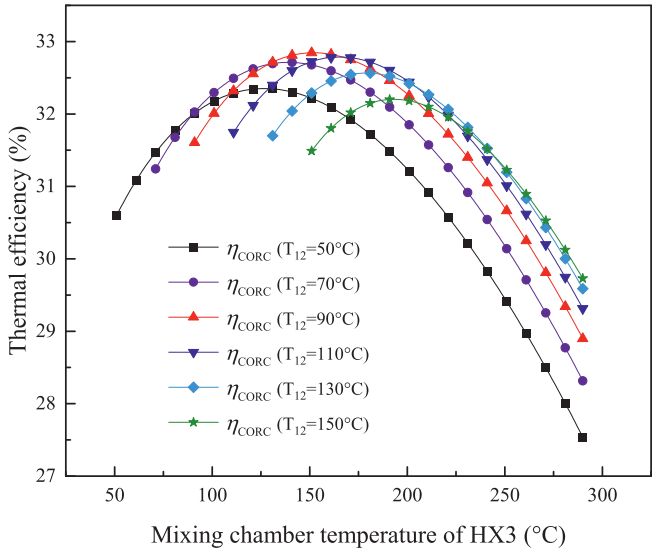

Fig. 13. Variation of the thermal efficiency of the CORC in Mode 1.

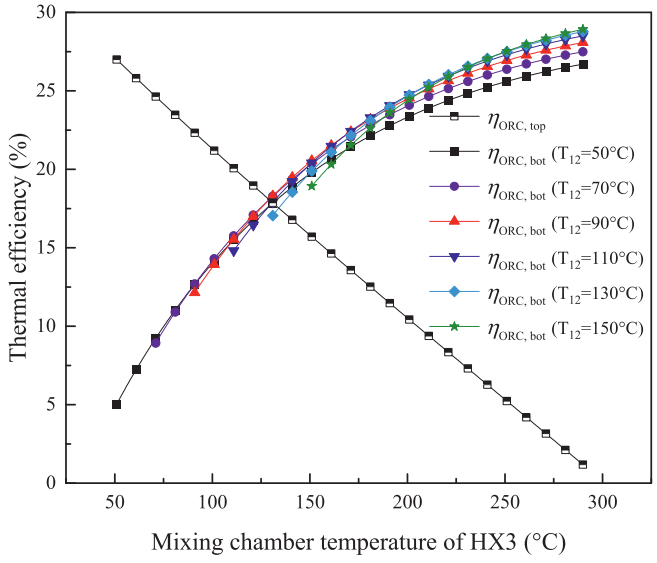

Fig. 14. Variation of the thermal efficiency of the top ORC and bottom ORC in Mode 1.

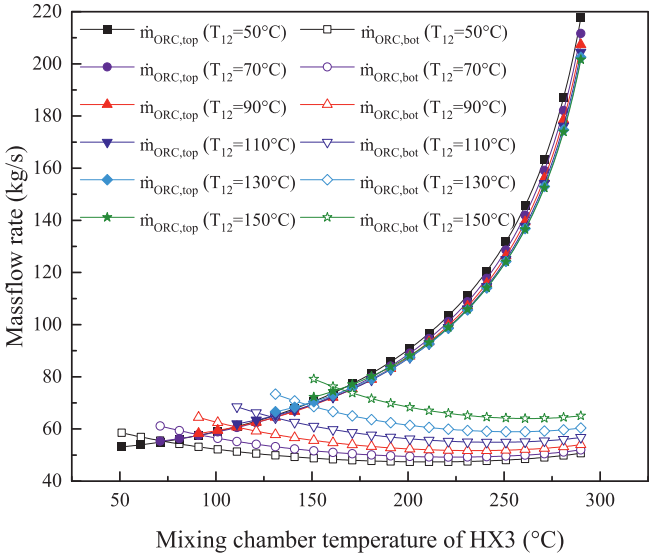

Fig. 15. Variation of the mass flow rate of the top ORC and bottom ORC in Mode 1.

Table 3
Parameters distribution at optimum CORC efficiency.

Point	T (°C)	h (kJ/kg)	P (MPa)	$\dot{m}$ (kg/s)	η_{CORC} (%)	$\eta_{ORC,top}$ (%)	$\eta_{ORC,bot}$ (%)
1	301.00	602.35	3.32	70.07	32.85	15.38	20.86
2	213.64	526.62	0.30	70.07			
3	173.62	454.55	0.30	70.07			
4	154.00	90.71	0.30	70.07			
5	155.71	95.85	3.32	70.07			
6	188.02	167.91	3.32	70.07			
7	154.00	420.76	0.30	56.02	W_{CORC} (MW)	$W_{ORC,top}$ (MW)	$W_{ORC,bot}$ (MW)
8	117.36	372.88	0.0598	12.32	10	4.68	5.32
9	67.11	305.59	0.0049	43.70			
10	30.00	149.69	0.0049	43.70			
11	30.02	−149.61	0.0598	43.70			
12	93.00	−34.69	0.0598	56.02			
13	93.11	−34.31	0.30	56.02			

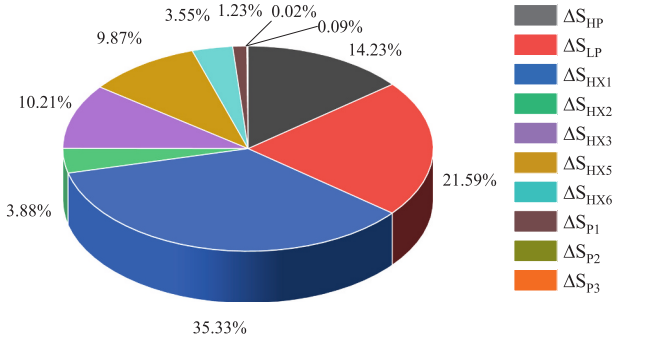

Fig. 16. Entropy generation of CORC at the maximum efficiency in Mode 1.

$$\Delta S_{P4} = S_{17} - S_{16} \quad (37)$$

4. Results and discussion

In this study, the following parameters are considered. The water/steam leaving the solar field has a temperature and pressure of 311 °C

Table 4
Parameters distribution at optimum CORC efficiency under different evaporation temperatures.

T_1 (°C)	T_4/T_7 (°C)	T_{12} (°C)	$W_{ORC,top}$ (MW)	$W_{ORC,bot}$ (MW)	$\eta_{ORC,top}$ (%)	$\eta_{ORC,bot}$ (%)	η_{CORC} (%)
285	150	91	4.68	5.32	15.12	20.45	32.30
290	151	92	4.69	5.31	15.26	20.55	32.50
295	152	92	4.70	5.30	15.37	20.66	32.67
300	154	93	4.68	5.32	15.35	20.86	32.82
305	155	94	4.67	5.33	15.39	20.96	32.94
310	156	94	4.66	5.34	15.37	21.06	33.01
315	157	95	4.62	5.38	15.22	21.15	32.97

Table 5
Parameters distribution at optimum CORC efficiency under different condensation temperatures.

T_{10} (°C)	T_4/T_7 (°C)	T_{12} (°C)	$W_{ORC,top}$ (MW)	$W_{ORC,bot}$ (MW)	$\eta_{ORC,\ top}$ (%)	$\eta_{ORC,bot}$ (%)	η_{CORC} (%)
10	146	79	4.56	5.44	16.24	23.39	35.62
15	148	82	4.59	5.41	16.02	22.75	34.92
20	150	86	4.62	5.38	15.81	22.11	34.23
25	152	90	4.65	5.35	15.60	21.48	33.54
30	154	93	4.68	5.32	15.38	20.86	32.85
35	156	97	4.72	5.28	15.17	20.24	32.16
40	159	100	4.72	5.28	14.85	19.73	31.48
45	161	104	4.75	5.25	14.63	19.13	30.80
50	163	108	4.79	5.21	14.42	18.53	30.13

and 10 MPa in normal operation. The HTT has an operating temperature of 250 °C. The mass of storage water (M_w) is assumed to be 1500 tones. Other specific parameters in the simulation are shown in Table 2.

4.1. Thermodynamic performance of Mode 1

In Mode 1, electricity is generated by the cascade cycle in a wide range of solar radiation. Variations of the heat-to-power efficiency of the CORC with the mixing chamber temperature of HX3 (T_4 or T_7) are given in Fig. 13. At different temperatures in the feed-fluid heater (T_{12}), the thermal efficiency of the CORC all presents a trend of increasing first and then decreasing.

When T_{12} is 50 °C, 70 °C, 90 °C, 110 °C, 130 °C, and 150 °C, there is a maximum thermal efficiency of 32.35%, 32.71%, 32.84%, 32.79%, 32.57%, and 32.20%, and the corresponding temperature of the mixing chamber HX3 is 127 °C, 139 °C, 152 °C, 165 °C, 179 °C, and 193 °C, respectively. Considering the temperatures in the feed-fluid heater (T_{12}) and the temperature of the mixing chamber HX3 (T_4) comprehensively, the maximum thermal efficiency appears when T_{12} is 154 °C and T_4 is 93 °C, and its value is 32.85%. Variation of the thermal efficiency of the top ORC and bottom ORC in Mode 1 is depicted in Fig. 14. As the mixing chamber temperature of HX3 increases, the thermal efficiency of the top ORC decreases. On the contrary, the thermal efficiency of the bottom ORC increases gradually. This is because when the net power output is fixed (10 MW), the power ratio of the top turbine to the bottom turbine decreases with the increment in T_4. When T_4 is 50 °C, 100 °C, 150 °C, 200 °C, and 250 °C, the thermal efficiency of top ORC is 27.00%, 21.31%, 15.81%, 10.53%, 5.34%, respectively. In addition, the higher the temperature of T_{12}, the more efficient the bottom ORC. Fig. 15 displays the mass flow rates of the top ORC and bottom ORC. With an increasing mixing chamber temperature of HX3, the mass flow rate of top ORC rises, while the value of bottom ORC decreases gradually. Details on parameters at different points (temperature, enthalpy, pressure, mass flow rates), work, and thermal efficiency (top ORC, bottom ORC, and CORC) at an optimum thermal efficiency of CORC are listed in Table 3.

Fig. 16 shows the thermodynamic irreversibility of the CORC at the optimum CORC efficiency. The entropy generation represents the exergy destruction. Since the temperature difference between the inlet steam in HX1 (311 °C) and the inlet ORC fluid (154 °C) is significant, the heat transfer destruction from water to the ORC fluid in HX1 is largest, accounting for 35.33% of the total exergy losses. The second and third largest exergy destructions are located at the bottom and top turbines (LP and HP) with values of 21.59% and 14.23%. The pumps contribute little to the entropy generation, where the entropy generation of pump P1 is 1.23%, the entropy generation produced by P2 and P3 is less than 1%.

The top ORC evaporation temperature plays an important role in the performance of the CORC system. As shown in Table 4, it influences the optimum temperatures of mixing chamber HX3 and HX5, and the maximum thermal efficiency of the CORC. As the evaporation temperature increases, the CORC and top ORC efficiencies first increase and then decrease. The optimum CORC efficiency and top ORC efficiency occur at evaporation temperatures of 310 °C and 305 °C with values of 33.01% and 15.39%, respectively. With the increasing evaporation temperature, the bottom ORC efficiency exhibits an upward trend. The results indicate that the CORC efficiency increment with the evaporation temperature is not appreciable. The reason is the ORC fluid is

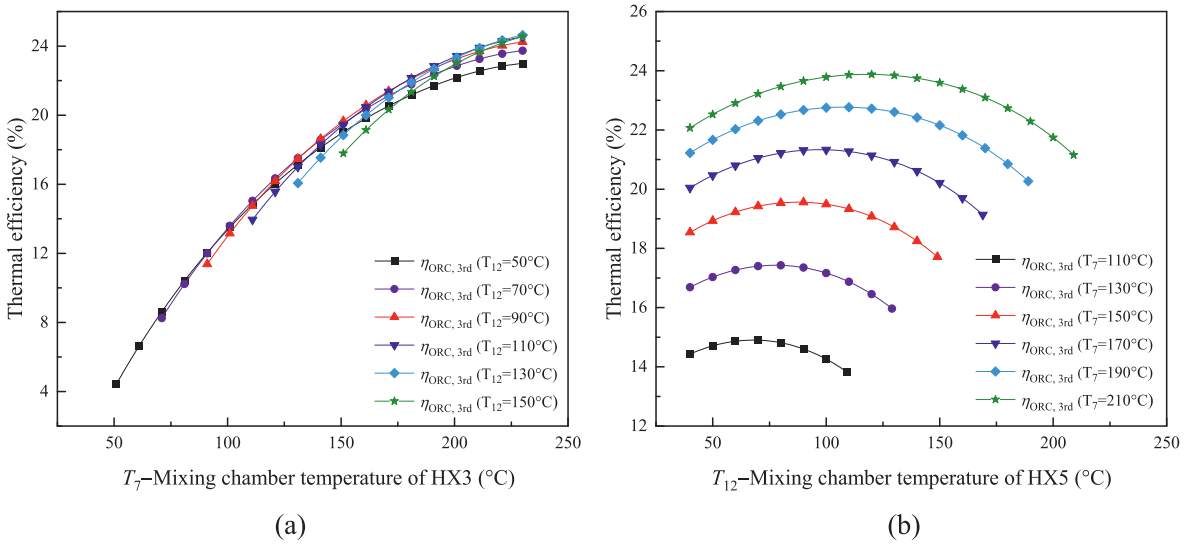

Fig. 17. Variation of the thermal efficiency of the bottom ORC in Mode 2 and Mode 5.

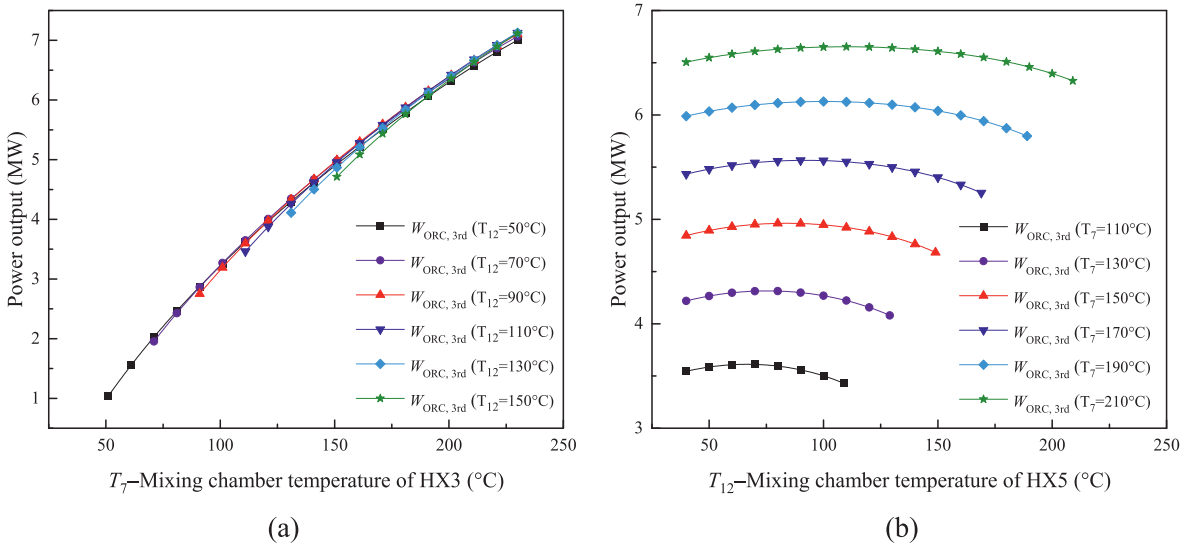

Fig. 18. Variation of the power output of the bottom ORC in Mode 2 and Mode 5.

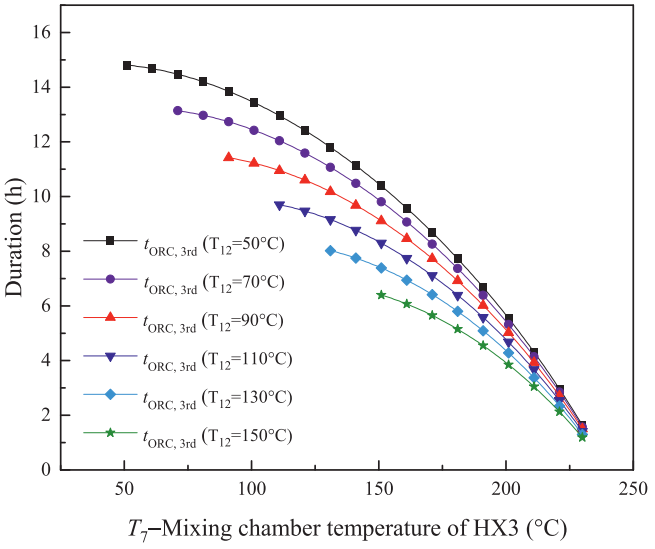

Fig. 19. Variation of heat discharge duration in Mode 2 and Mode 5.

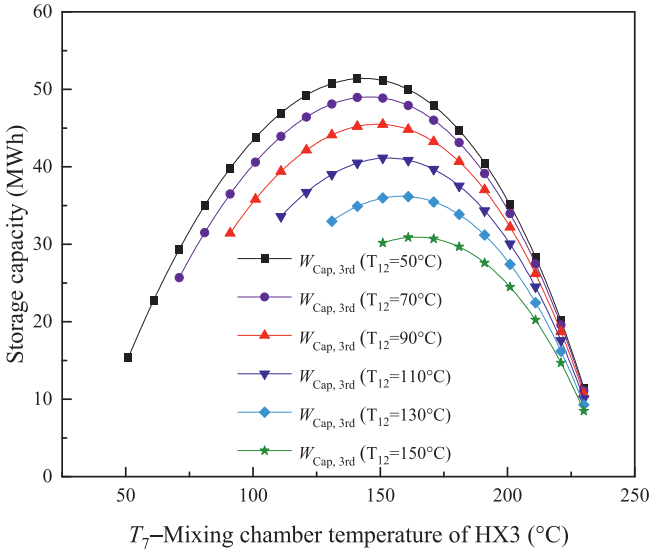

Fig. 20. Variation of heat storage capacity in Mode 2 and Mode 5.

approaching its critical temperature (318.64 °C) and it is a common phenomenon that the efficiency does not increase significantly with evaporation temperature near the critical point [14]. To further increase the CORC efficiency, fluids of higher critical temperature will be appreciated (e.g., biphenyl, diphenyl oxide, or mixture).

The influence of the condensation temperatures on the performance of the CORC system in the normal operation mode is also evaluated. Table 5 present the distribution of the parameters at maximum CORC efficiency under different condensation temperatures. The temperature at Point 10 (T_{10}) varies from 10 °C to 50 °C. The condensation temperature is related to the ambient temperature. As the condensation temperature decreases, the efficiencies of top ORC, bottom ORC, and CORC all show an increasing tendency. When T_{10} is 10 °C, the optimum CORC efficiency is as high as 35.62%.

4.2. Thermodynamic performance of Mode 2 and Mode 5

The variation of the thermal efficiency under different mixing chamber temperatures of HX5 in the simultaneous heat collection and bottom ORC power conversion mode and the third heat discharge mode is displayed in Fig. 17. T_7 and T_{12} have direct impacts on the performance of the bottom ORC. In addition, T_7 affects the power consumption of pump P4, and thus it needs to be included as a parasitic load when calculating the thermal efficiency of the bottom ORC, and it is related to the temperature and pressure of the water in the LTT and HTT. As shown in Fig. 17 (a), the thermal efficiency of the bottom ORC generally rises as T_7 increases. There are intersections among the curves at different T_{12}, and Fig. 17 (b) gives the variation of thermal efficiency as T_{12} increases. For a given T_7, the thermal efficiency first increases and then decreases. When T_7 is 110 °C, 150 °C, and 210 °C, the maximum thermal efficiency is 14.90%, 19.56%, and 23.88% at T_{12} of 68 °C, 87 °C, and 118 °C, respectively. The corresponding power output of the bottom ORC is displayed in Fig. 18. The variations of the power output and thermal efficiency are consistent. The variation of power output with the temperature of T_7 ($T_7 = T_4$) of the bottom ORC is the same as that in Mode 1 since the bottom ORC cycle is part of the 10 MW system. As T_7 rises from 110 °C to 210 °C, the maximum power output increases from 3.61 MW to 6.65 MW.

In the heat discharge process, aside from the thermal efficiency and

Table 6
Parameters distribution at maximum storage capacity.

T_{12} (°C)	T_7 (°C)	α	$\eta_{ORC,3rd}$ (%)	$W_{ORC,3rd}$ (MW)	$\dot{m}_{ORC,3rd}$ (kg/s)	$\dot{m}_{water,bot}$ (kg/s)	$t_{ORC,3rd}$ (h)	$W_{Cap,3rd}$ (MWh)
50	143	0.07	18.31	4.68	49.17	37.93	10.99	51.42
70	147	0.14	19.15	4.86	51.90	41.31	10.09	49.02
90	148	0.21	19.36	4.90	55.90	44.86	9.29	45.49
110	154	0.28	19.76	5.05	60.65	51.20	8.14	41.13
130	158	0.34	19.67	5.11	67.20	58.81	7.09	36.22
150	164	0.40	19.51	5.19	75.48	69.99	5.95	30.31

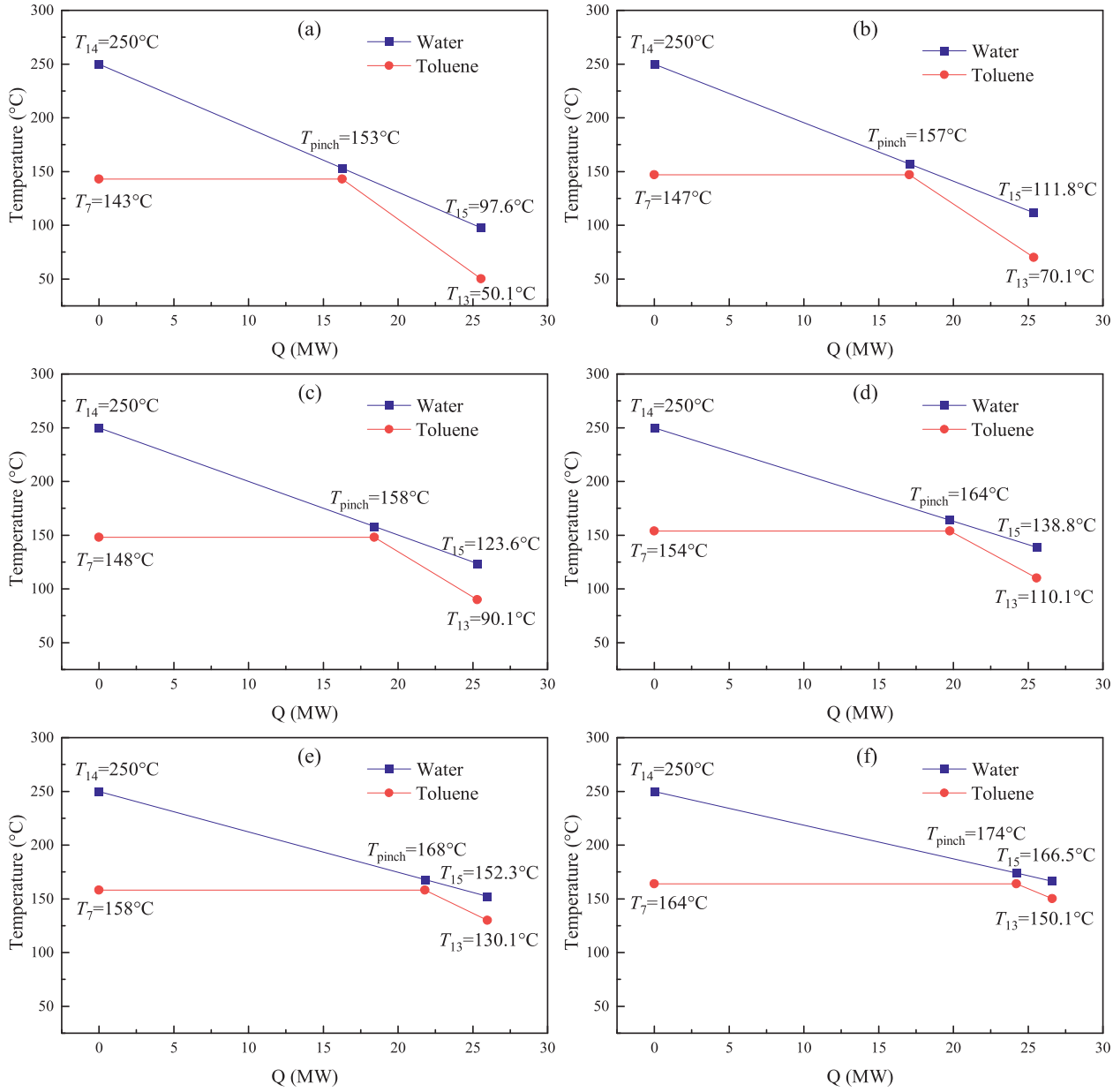

Fig. 21. T-Q diagrams of the HX4 in Mode 2 and Mode 5: (a) T_{12} = 50 °C; (b) T_{12} = 70 °C; (c) T_{12} = 90 °C; (d) T_{12} = 110 °C; (e) T_{12} = 130 °C; (f) T_{12} = 150 °C.

power output, the storage capacity is also an important indicator, which is affected by the water mass in HTT, inlet water temperature (T_7), and the mixing chamber temperature of HX5 (T_{12}). Variation of heat discharge duration in Mode 5 is shown in Fig. 19. As the temperature of T_7 or T_{12} increases, the duration is gradually shortened. Heat discharge duration decreases with the increase of T_7 due to the large power output and fast heat consumption. When T_{12} is below 110 °C and T_7 is less than 150 °C, the water mass of 1500 tons can result in a discharge duration from about 8 h to 15 h, and this seems desirable for the maximum annual power generation of 10 MW power plant.

Fig. 20 presents the variation of heat storage capacity in Mode 2 and Mode 5. There is a maximum value of heat storage capacity at different temperatures of mixing chamber HX5 (T_{12}). When T_{12} is 50 °C, 70 °C, 90 °C, 110 °C, 130 °C, and 150 °C, the maximum heat storage capacity

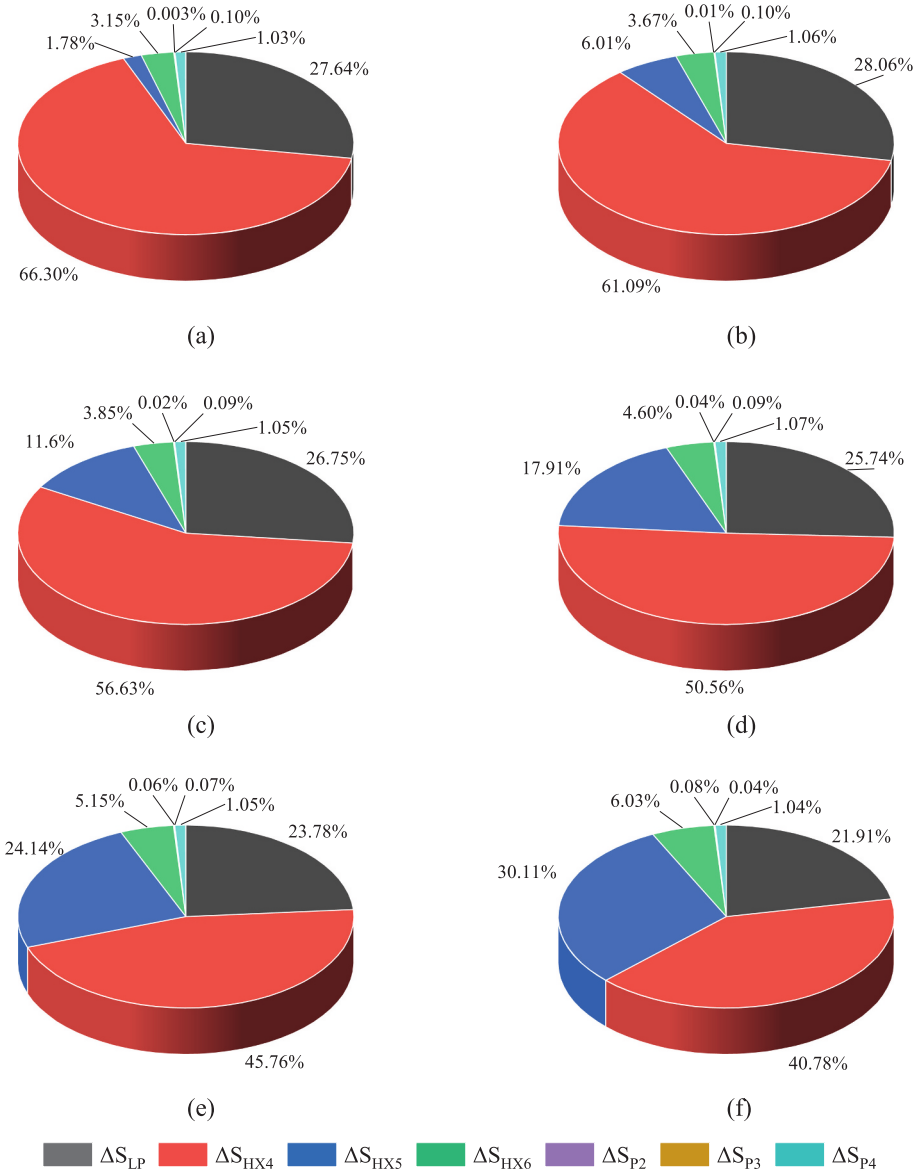

Fig. 22. Entropy generation of bottom ORC at maximum water storage capacity in Mode 2 and Mode 5:(a) $T_{12} = 50$ °C; (b) $T_{12} = 70$ °C; (c) $T_{12} = 90$ °C; (d) $T_{12} = 110$ °C; (e) $T_{12} = 130$ °C; (f) $T_{12} = 150$ °C.

with the water mass of 1500 ton is 51.42 MWh, 49.02 MWh, 45.49 MWh, 41.13 MWh, 36.22 MWh and 30.31 MWh with a corresponding T_7 of 143 °C, 147 °C, 148 °C, 154 °C, 158 °C, and 164 °C, respectively. The detailed parameters distribution at maximum storage capacity is shown in Table 6.

The T-Q diagrams in the third step of heat discharge are depicted in Fig. 21, which effectively reveals the relationship between fluid temperature and heat transfer rate in the HX4. The hot side water leaves the HTT at a constant temperature (T_{14}) but reaches the LTT at a different temperature (T_{15}). The minimum temperature difference occurs at the saturated liquid state, which is the pinch point ($T_{min} = 10$ °C).

Fig. 22 shows the thermodynamic irreversibility of the bottom ORC in Mode 2 and Mode 5. The heat transfer destruction from hot side water to the bottom ORC fluid in HX4 is largest, accounting for 60.30%, 61.09%, 56.63%, 50.56%, 45.76%, and 40.48% of the total exergy losses with a corresponding T_{12} of 50 °C, 70 °C, 90 °C, 110 °C, 130 °C, and 150 °C, respectively. This is followed by the exergy destructions at the bottom turbines (LP) and HX5. The exergy destruction of pump P4 is about 1.05% of the total exergy losses. The pumps P2 and P3 contribute little to the entropy generation with values less than 1%.

4.3. Thermodynamic performance of Mode 3

In Mode 3, the latent heat is released from the PCM to drive the CORC, and the CORC system operates at the off-design condition. The evaporation temperature of the organic fluid is likely to decrease due to the increased thermal resistance in the solidification process. Thus, the heat discharge capacity of PCM gradually decreases. To investigate the thermodynamic performance of the first heat discharge mode, the rated parameters of the CORC system are set, as shown in Table 3. Fig. 23 shows the variation of the power output ratio of the top ORC, bottom ORC, and CORC system in Mode 3 against the heat release ratio of PCM. It is defined as the ratio of the instant heat release rate from the PCM to the rated value. It is assumed to be 100% at the beginning of the first-step heat discharge and then drops as more and more PCM accumulates on the heat exchanger. When the heat release ratio decreases from 100% to 60%, the power output ratios of top ORC, bottom ORC, and CORC drop linearly from 100% to 56.82%, from 100% to 49.51%, and from 100% to 52.93%, respectively. The decrement in the heat release ratio not only reduces the total heat input to the CORC, but also leads to lower turbine and cycle efficiencies. Fig. 24 presents the variations of the

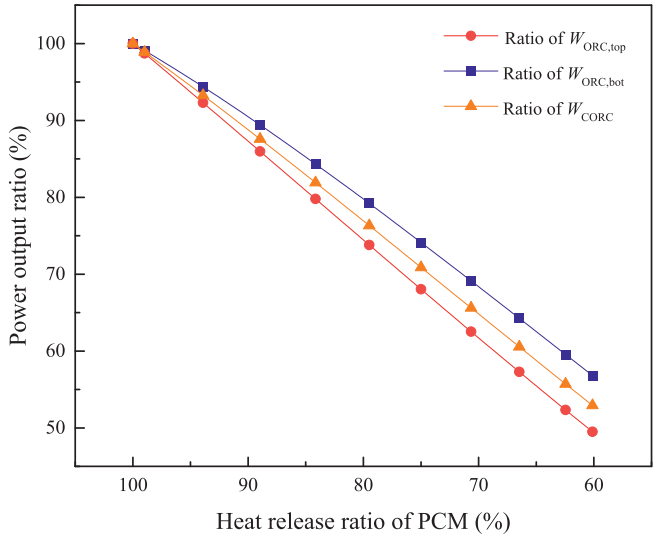

Fig. 23. Variation of the power output ratio of CORC system in Mode 3.

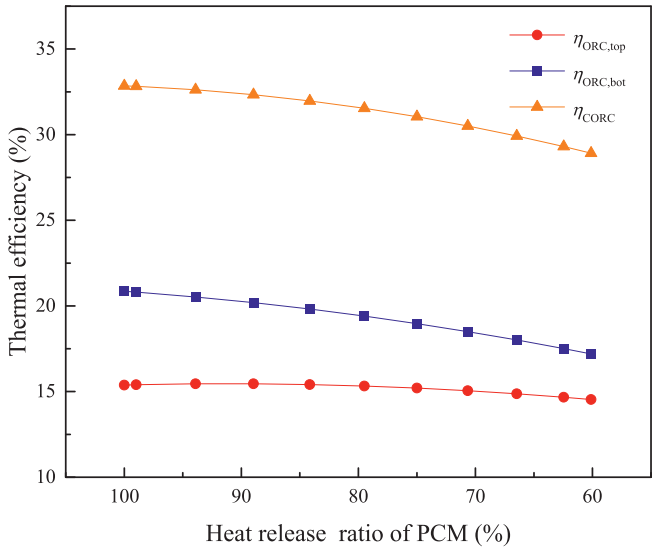

Fig. 24. Variation of the thermal efficiency of the top, bottom ORC, and CORC in Mode 3.

thermal efficiencies of the top, bottom ORC, and CORC in Mode 3. The thermal efficiencies generally decline with a decreased PCM heat release ratio. When the ratio is 100%, 80%, and 60%, the thermal efficiency of the CORC is 32.85%, 31.54%, and 28.92%, respectively.

4.4. Thermodynamic performance of Mode 4

In the second step of heat discharge, when the heat release ratio of PCM drops to 60%, the water in the HTT flows into the LTT. Therefore, HX4 compensates for the heat shortage from the PCM and guarantees the rated output of the bottom ORC. The temperature at Point 7 is maintained at 154 °C according to the rated parameters in Table 3. As shown in Fig. 25, when the heat discharge ratios of PCM are 60%, 50%, and 40%, the power output ratios of and CORC system are 76.00%, 70.21%, and 64.81%, which are all higher than that (56.82%) when the heat release ratio is 60% in Mode 3. From this, it can be seen that this design can alleviate the problems of insufficient heat release from PCM during discharge and keep a relatively high level of power output. Besides, the variations of the thermal efficiency and bottom water mass

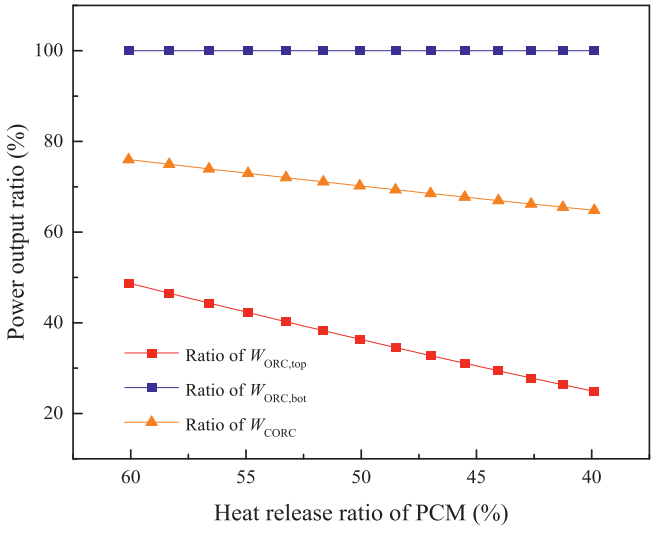

Fig. 25. Variation of the power output ratio of CORC system in Mode 4.

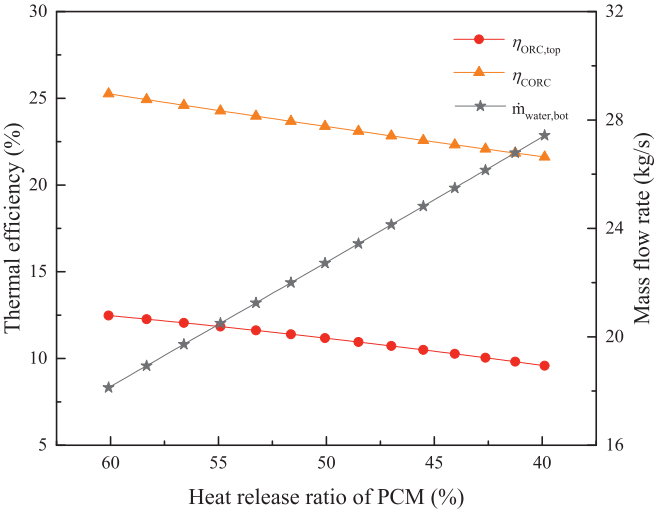

Fig. 26. Variations of the thermal efficiency and bottom water mass flow rate in Mode 4.

flow rate in HX4 are also given in Fig. 26. As the ratio decreases from 60% to 40%, the thermal efficiencies of top ORC and CORC descend from 12.48% to 9.58% and from 25.26% to 21.62%, respectively. Since the latent heat released from the PCM is in decline, the heat transferred from the top ORC to the bottom ORC through the mixing chamber HX3 is also reduced. Therefore, to ensure the rated output of the bottom ORC, more heat needs to be obtained from the bottom water through HX4. It can be seen from Fig. 26 that the mass flow rate of the bottom water is gradually increasing. Specifically, when the ratios are 60%, 50%, and 40%, the mass flow rates each are 18.13 kg/s, 22.72 kg/s, and 27.43 kg/s.

5. Economic advantages

Investigation of the levelized cost of electricity for the proposed system will be complicated. It will involve hypotheses in calculating the annual electricity output, capital cost, maintenance & repair cost. For a brief assessment of the economic performance, comparisons with conventional DSG and solar ORC systems are made below.

Conventional DSG systems have a limited storage capacity, as

Table 7
Some operational solar ORC plants worldwide [6].

Project name	Location	Type	Solar field temperature (°C)	Heat transfer fluid	Storage duration	Power capacity (MW)
Rende CSP Plant	Calabria Italy	LFC	in: 160 out:280	Diathermic oil	No heat storage	1
eLLO Solar Thermal Project	Occitanie France	LFC	in: 190 out:285	Water	3 h Steam drum	9
Aalborg CSP-Brønderslev CSP	North Jutland Denmark	PTC	in: 252 out:312	Biphenyl/diphenyl oxide	No heat storage	5.5
CSP-ORC PLUS	Benguerir Morocco	LFC	in: 180 out:300	Delcoterm Solar E15	4 h Magnetite ore	1

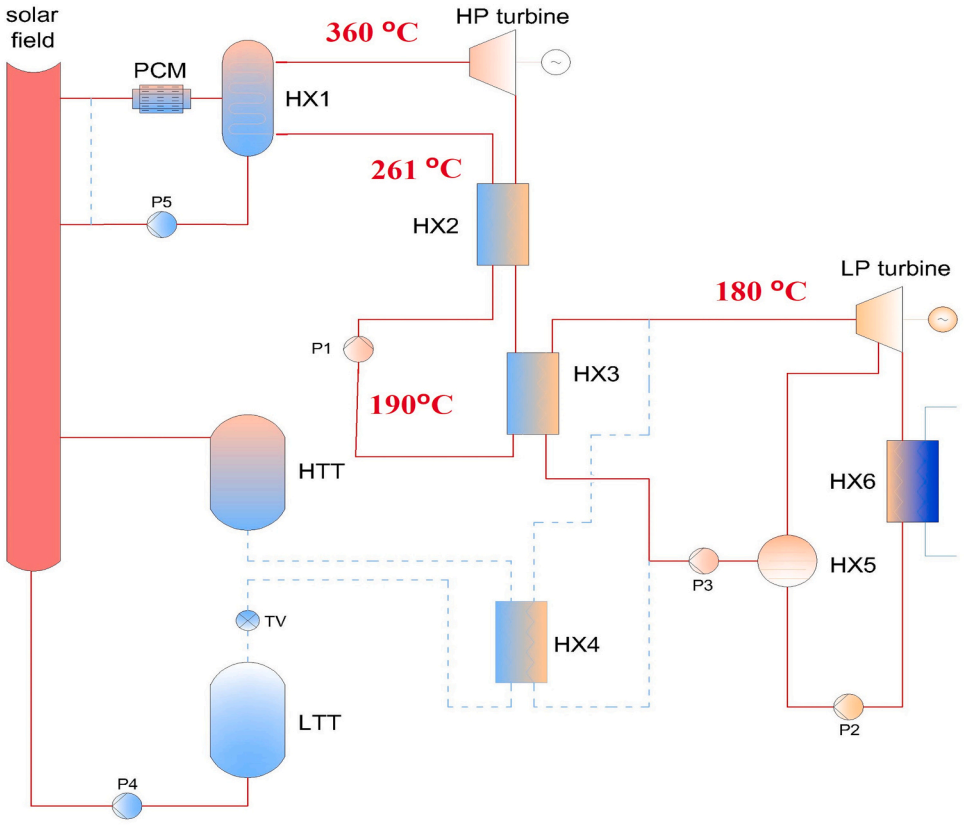

Fig. 27. High-temperature solar cascade organic Rankine cycle system using biphenyl-diphenyl oxide mixture.

depicted in Table 1. The proposed system offers an enlarged storage capacity because of the unique discharge process (Mode 5). The temperature drop of water from the HTT to LTT can exceed 150 °C, significantly larger than that in a conventional DSG discharge process. The unique heat discharge leads to an increased annual electricity yield. Given the steam generation temperature, rated power output, and accumulator volume, the proposed system has more solar collectors than conventional systems for the enlarged storage capacity. Its investment in dry ORC turbines is expected to be lower than in wet steam turbines. The solar collector cost is generally less than 50% of the total system cost, while the power efficiency in the discharge process is higher than 60% of the rated efficiency. Therefore, the proposed system can have a shorter payback time even if its steam generation temperature is the same as that of a common DSG. The payback time will drop further with the increment in the steam generation temperature, especially for a central receiver, owing to the increased efficiency in the normal operation (Mode 1).

Compared to conventional solar ORC systems, a shorter payback time is also anticipated. Some operational plants are listed in Table 7. They use linear Fresnel reflectors and parabolic trough collectors to harness solar energy, thermal oil and water to carry away and store the solar heat, and ORC to generate power. The fluid in the solar field is in a liquid state. The fluid temperature at the outlet of the solar field is 280–312 °C. Rende and Aalborg CSP plants are combined with biomass boilers and no thermal storage is adopted. The temperature at the inlet varies more remarkably and is usually lower when heat storage is employed. The ORC evaporation temperature is close to the solar field inlet temperature as the latent heat for evaporation is generally dominant in the heating process. The storage capacity is 3–4 h. More details on the plants' operation have yet to be published. The heat-to-power conversion of these plants should be similar to Mode 5 (heat discharge) in the proposed system, assuming the LTT and HTT temperature are equal to the solar field inlet and outlet temperature. The proposed system can be therefore deemed as a combination of a top ORC and a conventional solar ORC. The top ORC has an evaporation temperature slightly lower than the steam generation temperature (solar field outlet temperature). Compared with the conventional solar ORCs, the proposed system uses a top ORC turbine and heat exchangers to increase the solar electricity efficiency in the normal operation, thereby generating more electricity at a given solar field area and storage mass.

Assuming the top turbine has a power capacity of about 5 MW (700 $/kW) and an annual operation time of 3000 h, the equivalent payback time regarding the employment of the top ORC is less than 3 years.

6. Future work

The proposed system has the potential to operate at a higher temperature, e.g., >350 °C, thereby offering a higher heat-to-power conversion. The top ORC evaporation temperature in this work is restricted by the critical temperature of toluene. If the ORC fluid is replaced by a biphenyl-diphenyl oxide mixture, the efficiency will be elevated. The biphenyl-diphenyl oxide mixture is commonly known as thermal oil. It is widely used and has excellent thermal stability at temperatures up to 400 °C. It can be used in liquid, vapor or binary phase state. An example is presented in Fig. 27. Similar to the system in Fig. 4, steam is generated in the solar field but it is not the power cycle fluid. The bottom ORC fluid may still be toluene. However, the top ORC uses the biphenyl-diphenyl oxide mixture for power conversion. The steam generation temperature is 370 °C while the HTT temperature is still about 250 °C. Because the fluids of the top and bottom ORCs are different, there is no mixing chamber. Instead, a heat exchanger (HX3) is adopted. The preliminary simulation results show that, given a top ORC evaporation temperature of 360 °C and bottom ORC condensation temperature of 30 °C, the thermal efficiency of the system in Fig. 27 is about 38%. The efficiency will be comparable or higher than that of a conventional solar Rankine cycle. The water evaporation temperature in the conventional solar Rankine cycle ranges from about 265 to 330 °C depending on the solar field fluid (water, thermal oils or molten salts). The evaporation temperature and cycle efficiency are not high due to the large latent heat for water vaporization. The biphenyl-diphenyl oxide mixture can evaporate at a much higher temperature and is potentially more efficient. A comprehensive investigation will be conducted in the near future.

7. Conclusions

In this paper, a novel high-temperature solar CORC power generation system is proposed. The independent operation temperatures of the HP turbine and HTT enable a high thermal efficiency of the CORC but a low storage cost. The combination of sensible and latent heat storage units has the potential to overcome the challenge of PCM in the solar application, offering long-term, economical storage. The thermodynamic performance of the five operating modes at design and off-design conditions is analyzed. The effects of mixing chamber temperature, evaporation temperature of top ORC, and condensation temperature of bottom ORC are investigated.

In the normal operation, the thermal efficiency of the CORC first increases and then decreases with an increasing temperature of the mixing chamber. Given a top ORC evaporation temperature of 301 °C. A maximum CORC efficiency of 32.85% is achieved at an optimum mixing chamber temperature of 154 °C. The optimum mixing chamber temperature varies slightly with the top evaporation temperature while increasing almost linearly with the increment in the condensation temperature.

There are three steps in the discharge process. The PCM unit enables the first-step discharge and the water tanks guarantee the third-step discharge. In the second step, the sensible heat released by the hot water increases with the decrement in the latent heat released by the PCM. When the heat release rate of the PCM descends to 40% of the rated value, the power output of the CORC system only drops to 64.81%. The results show it is possible to maintain a high level of power output even at the final stage of PCM solidification.

In the future research, high-temperature ORC fluids such as biphenyl/diphenyl oxide mixture will be preferable to elevate the power cycle efficiency. As the evaporation temperature increases, a foreseeable challenge will be the huge steam pressure and the proposed system might not be able to use PTCs and LFCs. Water has a saturation pressure of more than 20 MPa at 370 °C. A replacement of water by the mixture is considerable. The mixture has a saturation pressure of merely 1.2 MPa at 400 °C. More research is needed to explore its potential in the solar ORC application.

CRediT authorship contribution statement

Xiao Ren: Data curation, Formal analysis, Software, Visualization, Investigation, Writing - original draft.

Jing Li: Conceptualization, Methodology, Formal analysis, Funding acquisition, Writing - Review & Editing.

Guangtao Gao: Visualization.

Gang Pei: Investigation.

Declaration of competing interest

We declare that we have no financial and personal relationships with other people or organizations that can inappropriately influence our work, there is no professional or other personal interest of any nature or kind in any product, service and/or company that could be construed as influencing the position presented in, or the review of, the manuscript entitled, “An innovative concentrated solar power system driven by high-temperature cascade organic Rankine cycle”.

Acknowledgements

The study was sponsored by the EU Marie Curie International Incoming Fellowships Program (703746) and Fundamental Research Funds of Central Universities (21CX06053A).

References

[1] C. Marugan-Cruz, S. Sanchez-Delgado, J. Gomez-Hernandez, D. Santana, Towards zero water consumption in solar tower power plants, Appl. Therm. Eng. 178 (2020), 115505.
[2] A.B. de Sa, V.C. Pigozzo, L. Tadrist, J.C. Passos, Direct steam generation in linear solar concentration: experimental and modeling investigation - a review, Renew. Sustain. Energ. Rev. 90 (2018) 910–936.
[3] L. Feng, H.P. Chen, Y.A. Zhou, S. Zhang, T.L. Yang, L.S. An, The development of a thermo-economic evaluation method for solar aided power generation, Energy Convers. Manag. 116 (2016) 112–119.
[4] E. Zarza, M.E. Rojas, L. Gonzalez, J.M. Caballero, F. Rueda, INDITEP: the first pre-commercial DSG solar power plant, Sol. Energy 80 (2006) 1270–1276.
[5] M. Eck, E. Zarza, Saturated steam process with direct steam generating parabolic troughs, Sol. Energy 80 (2006) 1424–1433.
[6] NREL, Concentrating Solar Power Projects. https://solarpaces.nrel.gov/2021.
[7] M.J. Montes, A. Rovira, M. Munoz, J.M. Martinez-Val, Performance analysis of an integrated solar combined cycle using direct steam generation in parabolic trough collectors, Appl. Energy 88 (2011) 3228–3238.
[8] A. Leyzerovich, Wet-steam Turbines for Nuclear Power Plants, PennWell Corporation, Tulsa, 2005.
[9] L. Xu, J.Q. Yuan, Online application oriented calculation of the exhaust steam wetness fraction of the low pressure cylinder in thermal power plant, Appl. Therm. Eng. 76 (2015) 357–366.
[10] T. Hirsch, A. Khenissi, A systematic comparison on power block efficiencies for CSP plants with direct steam generation, in: Proceedings of the Solarpaces 2013 International Conference 49, 2014, pp. 1165–1176.
[11] K. Baumann, Some recent developments in large steam turbine practice, J. Inst. Electr. Eng. 59 (1921) 565–623.
[12] E. Gonzalez-Roubaud, D. Perez-Osorio, C. Prieto, Review of commercial thermal energy storage in concentrated solar power plants: steam vs. Molten salts, Renew. Sustain. Energ. Rev. 80 (2017) 133–148.
[13] J. Li, P.C. Li, G.T. Gao, G. Pei, Y.H. Su, J. Ji, Thermodynamic and economic investigation of a screw expander-based direct steam generation solar cascade rankine cycle system using water as thermal storage fluid, Appl. Energy 195 (2017) 137–151.
[14] J. Li, J.Z. Alvi, G. Pei, Y.H. Su, P.C. Li, G.T. Gao, et al., Modelling of organic rankine cycle efficiency with respect to the equivalent hot side temperature, Energy 115 (2016) 668–683.
[15] S.I. Garcia, R.F. Garcia, J.C. Carril, D.I. Garcia, A review of thermodynamic cycles used in low temperature recovery systems over the last two years, Renew. Sustain. Energ. Rev. 81 (2018) 760–767.
[16] G.Q. Shu, L.N. Liu, H. Tian, H.Q. Wei, G.P. Yu, Parametric and working fluid analysis of a dual-loop organic rankine cycle (DORC) used in engine waste heat recovery, Appl. Energy 113 (2014) 1188–1198.

[17] F.H. Dubberke, M. Linnemann, W.K. Abbas, E. Baumhogger, K.P. Priebe, M. Roedder, et al., Experimental setup of a cascaded two-stage organic rankine cycle, Appl. Therm. Eng. 131 (2018) 958–964.
[18] G.T. Gao, J. Li, P.C. Li, H.L. Yang, G. Pei, J. Ji, Design and analysis of an innovative concentrated solar power system using cascade organic rankine cycle and two-tank water/steam storage, Energy Convers. Manag. 237 (2021), 114108.
[19] S. Sanaye, N. Khakpaay, Thermo-economic multi-objective optimization of an innovative cascaded organic rankine cycle heat recovery and power generation system integrated with gas engine and ice thermal energy storage, J. Energy Storage. 32 (2020), 101697.
[20] E. Ntavou, G. Kosmadakis, D. Manolakos, G. Papadakis, D. Papantonis, Experimental testing of a small-scale two stage organic rankine cycle engine operating at low temperature, Energy 141 (2017) 869–879.
[21] Z.X. Sun, J.P. Lai, S.J. Wang, T.L. Wang, Thermodynamic optimization and comparative study of different ORC configurations utilizing the exergies of LNG and low grade heat of different temperatures, Energy 147 (2018) 688–700.
[22] G.P. Yu, G.Q. Shu, H. Tian, H.Q. Wei, X.Y. Liang, Multi-approach evaluations of a cascade-organic rankine cycle (C-ORC) system driven by diesel engine waste heat: part B-techno-economic evaluations, Energy Convers. Manag. 108 (2016) 596–608.
[23] T. Chen, W.L. Zhuge, Y.J. Zhang, L. Zhang, A novel cascade organic rankine cycle (ORC) system for waste heat recovery of truck diesel engines, Energy Convers. Manag. 138 (2017) 210–223.
[24] T. Sung, K.C. Kim, Thermodynamic analysis of a novel dual-loop organic rankine cycle for engine waste heat and LNG cold, Appl. Therm. Eng. 100 (2016) 1031–1041.
[25] I.H. Choi, S. Lee, Y. Seo, D. Chang, Analysis and optimization of cascade rankine cycle for liquefied natural gas cold energy recovery, Energy 61 (2013) 179–195.
[26] A. Sadreddini, M.A. Ashjari, M. Fani, A. Mohammadi, Thermodynamic analysis of a new cascade ORC and transcritical CO2 cycle to recover energy from medium temperature heat source and liquefied natural gas, Energy Convers. Manag. 167 (2018) 9–20.
[27] M. Leveni, R. Cozzolino, Energy, exergy, and cost comparison of goswami cycle and cascade organic rankine cycle/absorption chiller system for geothermal application, Energy Convers. Manag. 227 (2021), 113598.
[28] P.C. Li, J. Li, G. Pei, A. Munir, J. Ji, A cascade organic rankine cycle power generation system using hybrid solar energy and liquefied natural gas, Sol. Energy 127 (2016) 136–146.
[29] G.T. Gao, J. Li, P.C. Li, J.Y. Cao, G. Pei, Y.N. Dabwan, et al., Design of steam condensation temperature for an innovative solar thermal power generation system using cascade rankine cycle and two-stage accumulators, Energy Convers. Manag. 184 (2019) 389–401.
[30] D. Verez, E. Borri, A. Crespo, B.D. Mselle, A. de Gracia, G. Zsembinszki, et al., Experimental study on two PCM macro-encapsulation designs in a thermal energy storage tank, Appl. Sci.Basel. 11 (2021) 6171.
[31] J. Lizana, C. Bordin, T. Rajabloo, Integration of solar latent heat storage towards optimal small-scale combined heat and power generation by organic rankine cycle, J. Energy Storage 29 (2020), 101367.
[32] P. Gang, L. Jing, J. Jie, Design and analysis of a novel low-temperature solar thermal electric system with two-stage collectors and heat storage units, Renew. Energy 36 (2011) 2324–2333.
[33] J. Freeman, I. Guarracino, S.A. Kalogirou, C.N. Markides, A small-scale solar organic rankine cycle combined heat and power system with integrated thermal energy storage, Appl. Therm. Eng. 127 (2017) 1543–1554.
[34] D. Laing, C. Bahl, T. Bauer, D. Lehmann, W.D. Steinmann, Thermal energy storage for direct steam generation, Sol. Energy 85 (2011) 627–633.
[35] C. Prieto, D.P. Osorio, E. Gonzalez-Roubaud, S. Fereres, L.F. Cabeza, Advanced concrete steam accumulation tanks for energy storage for solar thermal electricity, Energies 14 (2021) 3896.
[36] J. Li, G. Pei, Y.Z. Li, D.Y. Wang, J. Ji, Examination of the expander leaving loss in variable organic rankine cycle operation, Energy Convers. Manag. 65 (2013) 66–74.